PROCEEDINGS OF SPIE

SPIEDigitalLibrary.org/conference-proceedings-of-spie

Numerical and experimental study of the dynamics of cross polarization coupling in a whispering-gallery microresonator

Limu Ke, Sreekul Raj Rajagopal, A. T. Rosenberger

Limu Ke, Sreekul Raj Rajagopal, A. T. Rosenberger, "Numerical and experimental study of the dynamics of cross polarization coupling in a whispering-gallery microresonator," Proc. SPIE 10904, Laser Resonators, Microresonators, and Beam Control XXI, 109041T (4 March 2019); doi: 10.1117/12.2508018

SPIE.

Event: SPIE LASE, 2019, San Francisco, California, United States

Numerical and experimental study of the dynamics of cross polarization coupling in a single whispering-gallery microresonator

Limu Ke, Sreekul Raj Rajagopal, and A. T. Rosenberger*
Department of Physics, Oklahoma State University, Stillwater, OK, USA 74078-3072

ABSTRACT

The cross polarization coupling (CPC) between orthogonally polarized modes in a single whispering-gallery microresonator can lead to electromagnetically induced transparency (EIT) like effects. Depending on the CPC strength, coupled mode induced transparency (CMIT), coupled mode induced attenuation (CMIA), or Autler-Townes splitting (ATS) can be observed. Previously, the values of CPC strength were found by fitting the experimental throughput spectra to a steady-state model. However, our dynamical analysis suggests an independent way of estimating the CPC strength by sinusoidal modulation at the input. From experimentally determined parameters, we first find one estimate of the CPC strength by model fitting as before. From the modulation frequency that gives the minimum throughput amplitude on resonance, we find another estimate of the CPC strength. Our preliminary experimental results show that the two values agree quite well, which means we have an independent way of finding the CPC strength.

Keywords: microresonator, whispering-gallery modes, induced transparency, cross polarization coupling

1. INTRODUCTION

Whispering-gallery mode (WGM) microresonators are characterized by having ultrahigh-quality (Q) factors and small optical-mode volumes,[1] thereby making them advantageous for studies in areas such as cavity QED, nonlinear optics, optomechanics, and high-sensitivity sensing. Using WGM microresonators, we can also observe classical analogs of the electromagnetically induced transparency (EIT) effects in atomic systems where laser-induced coherence of atomic states leads to quantum interference between the excitation pathways that control the optical response.[2] In EIT, a narrow transparency window is created by eliminating a resonant absorption. Under the right conditions, electromagnetically induced absorption (EIA) can also take place. Induced transparency is generally accompanied by pulse delay (slow light), whereas induced absorption can show pulse delay or pulse advancement (fast light).[3] Autler–Townes splitting[4] (ATS) also displays a transparency window (similar to EIT). However, ATS is not the result of interferences[5] but involves field-induced splitting of energy levels. Recent theoretical analysis of coupled microresonators[6] has revealed that coherence effects in the coupled resonator system are remarkably similar to those in atoms. Experimental observation of induced transparency and absorption in coupled microspheres[7] has also been reported. Due to the evanescent coupling between the coresonant WGMs of the two microspheres, the net throughput power in the coupled resonator system has features analogous to the EIT and EIA phenomena. This is accounted for by the destructive or constructive interference between the coresonant WGMs of the two microresonators, which either reduces or enhances light losses in the system, resulting in coupled resonator induced transparency (CRIT) or coupled resonator induced attenuation (CRIA) effects.

Induced transparency can also be observed in a single microresonator by several methods,[8] one of which involves cross-polarization coupling[9] (CPC) where light of one polarization circulating in a WGM of the microresonator can be coupled into a coresonant WGM of the orthogonal polarization. This CPC is likely a result of weak polarization rotation.[10] In this case, the input light and detected throughput is one polarization, say TE (transverse electric). Because of CPC, the interaction with a coresonant TM (transverse magnetic) WGM produces a throughput spectrum (as the driving laser is scanned in frequency) showing cross-polarization coupled-mode induced transparency and attenuation (CMIT, CMIA), observed as splitting or modification of the shape of the resonant dip.[11] To get a better understanding of CPC, we need to determine the value of the intermode coupling strength, which was inferred from fitting the experimental data to a steady-state computer model in other experiments. Our dynamic studies proposed here provide an independent measurement of the strength of the CPC that makes IT and IA possible.

*atr@okstate.edu; phone 1 405 744-6742; fax 1 405 744-6811; physics.okstate.edu/rosenber/index.html

Laser Resonators, Microresonators, and Beam Control XXI, edited by Alexis V. Kudryashov, Alan H. Paxton, Vladimir S. Ilchenko, Proc. of SPIE Vol. 10904, 109041T · © 2019 SPIE
CCC code: 0277-786X/19/$18 · doi: 10.1117/12.2508018

2. MODEL ANALYSIS OF CPC

2.1. Ring cavity model

To get a physical understanding of the dynamics of CPC and the resultant CMIT/CMIA effects, we can use a ring cavity model as shown in Fig. 1. In the model, the CPC between the intracavity circulating TE and TM modes is treated as a cross-polarization rotation with amplitude $\pm t_s$ near the input/output coupling point. Two input fields (actually, the TE and TM components of a single input field) are injected into the resonator, where they couple to each other. The net reflected fields are analogous to the throughput fields in a whispering-gallery microresonator system. The labeled fields and other system parameters are defined and discussed in the following text.

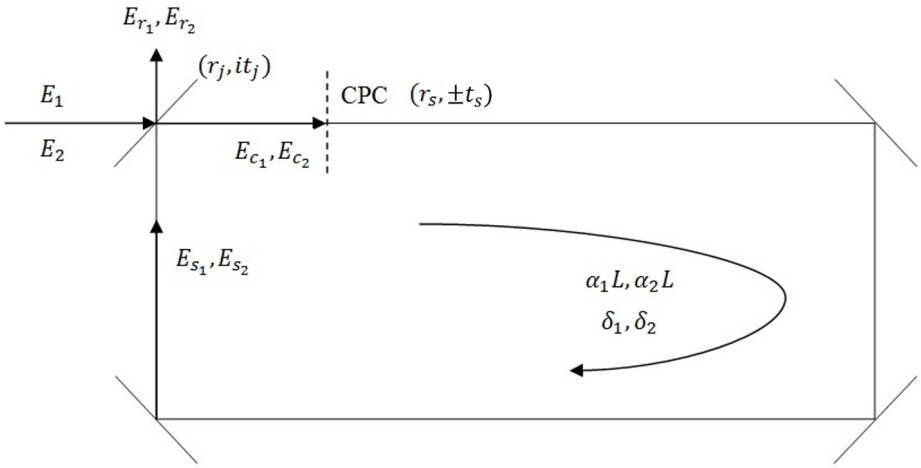

Fig. 1. Ring cavity model.

In the model, E_j (j = 1, 2) are orthogonal polarization components of the input field. One of the four mirrors is a partially transmitting mirror with reflection and transmission coefficients r_j and it_j, while the other three mirrors are perfectly reflective. The partial reflector is assumed to be ideal, so that $R_j + T_j = 1$, where $R_j = r_j^2$ and $T_j = t_j^2$. The intracavity fields of the two orthogonally polarized modes just before and just after the input/output coupler are E_{s_j} and E_{c_j}, respectively. With CPC just after the coupler, we assume round-trip losses of $\alpha_j L$ and round-trip phase shifts δ_j.

2.2. Analytical analysis of CPC

We assume that changes in a round trip are small, so that the steady-state equations for the intracavity fields E_{s_j} can be converted into a coupled set of first-order differential equations, where relations between the coefficients and total (complex) loss rate γ_j are given by

$$\gamma_j = \frac{T_j + \alpha_j L}{2\tau_{rt_j}} - i\frac{\delta_j}{\tau_{rt_j}} + \frac{T_s}{2\tau_{rt_j}} = \kappa_j(1 + i\theta_j) + \frac{T_s}{2\tau_{rt_j}}, \tag{1}$$

where $T_s = t_s^2 = 1 - r_s^2$ is the cross coupling probability per round trip, and is the measure of CPC strength; τ_{rt_j} is the round trip time; the field decay rate is $\kappa = (T_j + \alpha_j L)/2\tau_{rt_j} = 1/2\tau_j$, where τ_j is the photon lifetime for mode j; and θ_j is the detuning of the resonant frequency of mode j from the input frequency, in units of half the mode linewidth. The cross-polarization coupling to the orthogonal mode comes in as an additional "intrinsic" loss. Note that the quality factor of mode j can be written as $Q_j = \omega_j\tau_j = \omega_j/2\kappa_j$, where ω_j is mode j's resonant frequency. Now using $E_{r_j} = r_j E_j + itE_{s_j}$ gives first-order and second-order differential equations for the throughput fields. Then, if we assume the CPC strength T_s is very small and both modes are driven on resonance ($\theta_j = 0$), so $\gamma_j \approx \kappa_j$, the second-order differential equation for the

intracavity fields E_{s_j} takes the form of a damped driven oscillator. In the case of no driving, input fields $E_1 = E_2 = 0$, we can try $E_{s_1} \propto e^{-\beta t}$ and get an expression for the complex decay constants of the supermodes:

$$\beta_{\pm} = \frac{\kappa_1 + \kappa_2}{2} \pm \sqrt{(\frac{\kappa_1 - \kappa_2}{2})^2 - \frac{T_s}{\tau_{rt_1}\tau_{rt_2}}} \,. \tag{2}$$

Then for weak (but non-negligible) intermode coupling: $T_s / \tau_{rt_1}\tau_{rt_2} < [(\kappa_1 - \kappa_2)/2]^2$, the radicand is positive and gives two real values for $\beta_{\pm}$ and the destructive interference between the direct and indirect excitation paths of the intracavity field produces the CMIT feature of the throughput power. In contrast, if the coupling is made strong enough: $T_s / \tau_{rt_1}\tau_{rt_2} > [(\kappa_1 - \kappa_2)/2]^2$, the radicand becomes negative, gives two complex values for $\beta_{\pm}$, and the throughput now exhibits ATS. The radicand being zero defines the exceptional point.

Consider the case of one component where that component is the only input and might be sinusoidally modulated in amplitude at frequency Ω as follows: $E_1 = A_1 e^{-i\Omega t}$, $E_2 = 0$. Then we have, for $E_{s_1} = A_{s_1} e^{-i\Omega t}$:

$$A_{s_1} = \frac{(\Omega + i\kappa_2)\frac{t_1}{\tau_{rt_1}} A_1}{\Omega_0{}^2 - \Omega^2 - i\Omega(\kappa_1 + \kappa_2)} \tag{3}$$

where $\Omega_0{}^2 = \kappa_1\kappa_2 + T_s / \tau_{rt_1}\tau_{rt_2}$, and leads to a way of determining the CPC coupling strength T_s.

2.3. Numerical analysis of CPC

The ring cavity model described above has been incorporated into a Mathematica program for calculation of CMIT/CMIA behavior (intermode CPC). In the program, typical experimental parameter values are input, and the cross-polarization coupling strength is treated as an adjustable parameter. The output coupling and intrinsic loss are adjusted indirectly by giving the values of the quality factor *Q* of each mode (determines total loss), of the depth *M* of each mode's resonance dip (determines ratio of losses), and of the coupling regime (allows determination of each loss independently). The coupling regimes are overcoupled (coupling loss greater), undercoupled (intrinsic loss greater), and critical (losses equal).

The model has previously been used to study fast and slow light in CMIT/CMIA by modulating the input with a Gaussian pulse.[11] Here, the input amplitude is sinusoidally modulated to see throughput modulation amplitude and phase shift. With sinusoidal input, there will be an obvious phase shift and the amplitude is not just the zero-detuning value of the throughput power. We will see the occurrence of sidebands and the attenuation on the throughput amplitude can be strong or weak depending on the modulation phase shift relative to the input.

We plotted the throughput modulation amplitude and phase vs. modulation frequency Ω for a number of cases of CMIT/CMIA and ATS. We discovered from the near coincidence of the frequency of minimum modulation amplitude with the frequency of zero phase (at least for CMIT and ATS) that when the two *Q*s are very different, specifically when $Q_2 >> Q_1$ (so $\kappa_2 << \kappa_1$), the intermode coupling strength T_s is determined only by the modulation frequency at minimum amplitude, $\Omega_{\min}$, from the following approximation:

$$\Omega_{\min}{}^2 = \Omega_0{}^2 - \kappa_2(\kappa_1 + \kappa_2) \approx \Omega_0{}^2 - \kappa_1\kappa_2 = \frac{T_s}{\tau_{rt}{}^2} \,. \tag{4}$$

To illustrate this, we looked at a case of typical CMIT from the model, where the parameter values chosen are experimentally realistic.[11] For this case of CMIT the coupling strength is $T_s = 5\times10^{-8}$. We wrote a separate Mathematica program that calculates the modulation frequency $\Omega_{\min}$ at the minimum modulation amplitude. For our CMIT with $T_s = 5\times10^{-8}$, the program gives $\Omega_{\min} = 2.36\times10^7\ s^{-1}$. And then with minimal perturbation to our CMIT feature and keeping the two *Q*s very different, we tried in the ring cavity model a range of different values of T_s and calculated $\Omega_{\min}$ for each case. The square of the calculated values of $\Omega_{\min}$ has a near proportional dependence on T_s just as in Eq. (4) in our numerical model investigation. We continued with a case of ATS where the parameter values are the same as our CMIT but with a larger T_s. In the ring cavity model, choosing $T_s = 10^{-6}$ gave us an ATS feature, for which our new program

gives $\Omega_{min} = 1.1\times10^{8}\ s^{-1}$. Again, while keeping the ATS feature and two different Qs, we tried another range of different values of T_s and calculated the corresponding values for Ω_{min} in each case. The square of the calculated values of Ω_{min} also has a near proportional dependence on T_s. Fig. 2 shows the relation between T_s and Ω_{min}^2 for both cases.

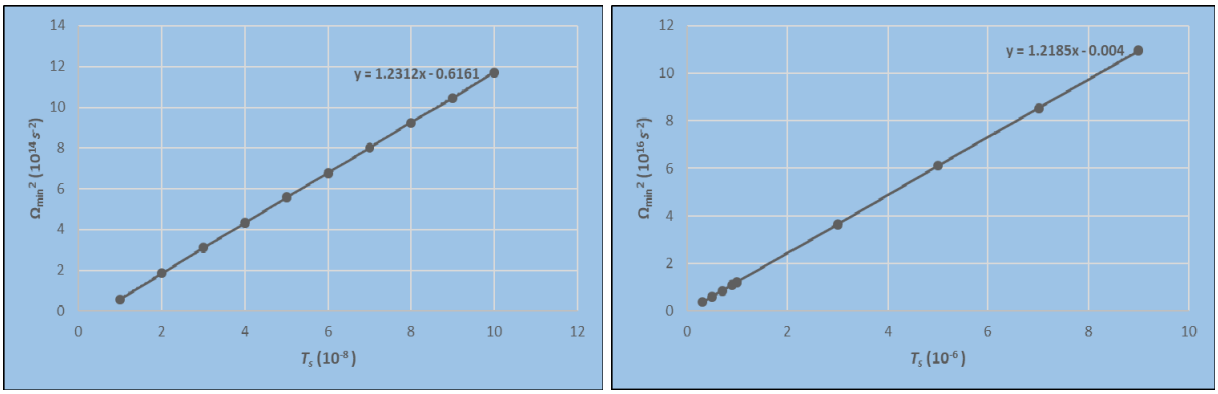

Fig. 2. Near proportional dependence of T_s on Ω_{min}^2 (left: CMIT; right: ATS).

Both graphs are linear, meaning that our approximation in Eq. (4) in numerical analysis is reasonable, at least for CMIT and ATS where the two Qs are very different. In the graphs, the y-intercept represents the difference between the true values of Ω_{min}^2 and our approximation in Eq. (4), namely κ_2^2. For our cases, however, this difference can be neglected since $\kappa_2 << \kappa_1$. Then we can establish a direct proportional relation between Ω_{min}^2 and T_s. Our numerical investigation leads us to think that, experimentally, by only finding the modulation frequency corresponding to minimum modulation amplitude, we should be able to directly estimate the CPC strength without the need to fit to a computer model.

3. EXPERIMENTAL RESULTS

3.1. Experimental setup

The experimental setup we used is shown in Fig. 3. The tunable diode laser (λ = 1508-1662 nm) is scanned in frequency by a function generator (FG1). The free-space output beam from the laser head passes through an anamorphic prism (AP) and optical isolator (OI). An acousto-optic modulator (AOM), controlled by function generator FG2, is then used to split the incoming beam into two outgoing parts: the zeroth-order undeflected beam of higher intensity with the same frequency and direction; and the first-order deflected beam of lower intensity with different frequency and direction from the incoming beam (which is used for amplitude modulation). Before going to the fiber coupler (FC), the deflected light beam passes through a set of wave plates (WP) which are used to control the input polarization. Usually, the wave plates are adjusted to provide linearly polarized light. The fiber coupler FC launches the light into a single mode fiber. The fiber isolator, acting as an optical diode, is used to prevent any backward propagating light. The single mode fiber is also mounted in a compression based polarization controller, PC, for further regulation of the input light. The region of the fiber after PC is kept short and straight to preserve the polarization.

We use a hollow-bottle microresonator[12] (HBR), instead of a silica microsphere, in our experiments. Due to its bottle shape, the HBR has some advantages over the microsphere for controlling the cross polarization coupling. Bottle resonators provide the benefits of high Q, tunability (by stretching), axial mode confinement, and mode selectivity (by positioning the coupling fiber). A WGM in an HBR is described by three mode indices: the azimuthal index m is the number of wavelengths in the circumference, the radial index p is the number of radial intensity maxima, and the axial index q is the number of axial field nodes. The WGMs of an HBR can be tuned easily by stretching the resonator, and the two polarizations tune at different rates, so coresonance can be imposed (rather than achieving it by coincidence). So it is easier to see CPC effects and study the resultant CMIT/CMIA with the help of HBRs. To make the HBR, a fused-silica capillary is internally etched with a hydrofluoric acid solution to thin its walls to a thickness of 5-10 μm, and then a

short length is heated using a hydrogen torch while under internal air pressure, leading to the formation of a bottle-shaped bulge.[13] The fiber is made adiabatically bi-tapered and brought into contact with the HBR in its equatorial plane using a 3D translation stage (not shown). The HBR is mounted on a piezo-controlled holder for strain tuning.

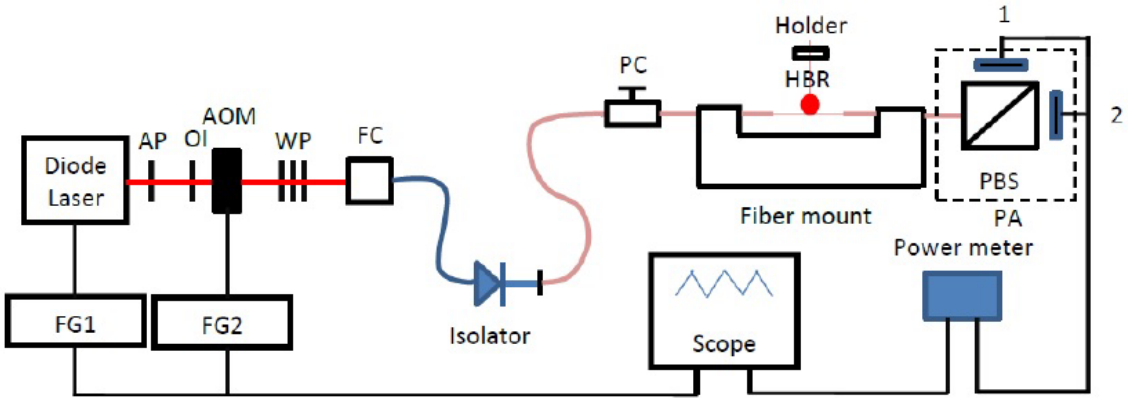

Fig. 3. Experimental setup.[11]

In all cases, the resonator is kept inside an acrylic box to minimize the temperature fluctuations and other effects of air movement. The output signal is sent to a fiber coupled polarization analyzer (PA) which includes the polarizing beam splitter (PBS) and two detectors, 1-fast detector and 2-slow detector, and can be rotated about the fiber axis so that either detector can detect either polarization. For data analysis, the signal on the slow detector is captured with the power meter and sent to the oscilloscope while the fast detector is directly connected to the oscilloscope.

3.2. Preliminary results

When only one polarization is driven at the input, strain tuning to coresonance and proper adjustment of the input polarization will result in the throughput spectrum consisting of the throughput power vs. scanned laser frequency: CMIT or ATS in our case. During the experiment, CPC can happen and make it difficult to determine the true values of the mode parameters like quality factors (Q), dip depths (M), and coupling regimes of the coresonant TE and TM modes. So in order to determine the mode parameters correctly, detuning the coresonant TE and TM modes is necessary. For a CMIT/ATS feature, we change the input polarization to 45° with respect to the microresonator's basis to show the throughput spectrum in both polarizations. Then we detune the resonance modes at this position and look at the individual modes in each polarization and measure the mode parameters. We use these individual mode parameters to fit the throughput spectrum to the model by adjusting the value of CPC strength in the model to get our first estimate of T_s. An example of numerical fitting for estimating the value of T_s is given in Fig. 4.

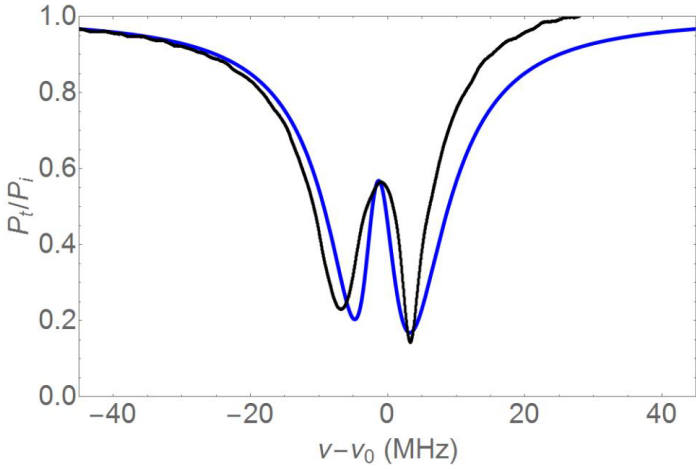

Fig. 4. CMIT with 175-um-radius HBR.[14] Experimental (black) and numerical fitting (blue) throughput spectra. Parameter values: $Q_1 = 1.1\times10^7$, $Q_2 = 9.5\times10^7$; $M_1 = 0.865$ (undercoupled), $M_2 = 0.42$ (overcoupled). From the fit to a steady-state model, it is found that $T_s = 1.51\times10^{-8}$.

After that, we carefully bring the two detuned modes back to resonance to retrieve our CMIT/ATS feature, and then we turn on the sinusoidal modulation to look at the response of the throughput spectrum. We vary the modulation frequency and record the amplitude of the modulated signal at different values. An example of the amplitude modulation for a CMIT feature at different modulation frequencies of the AOM is shown in Fig. 5.

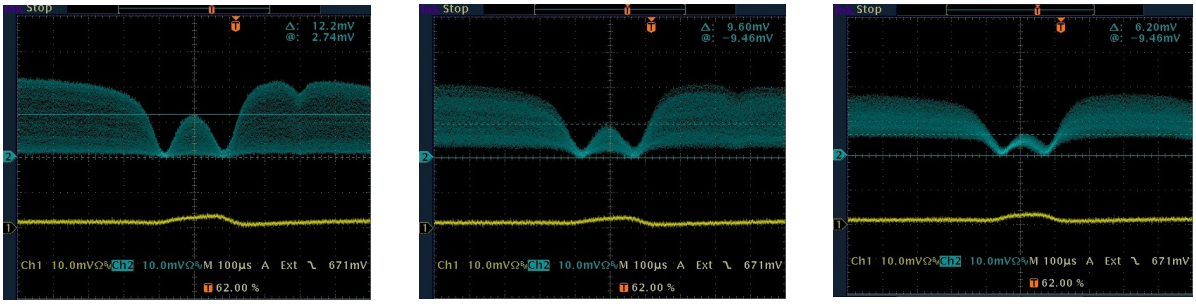

Fig. 5. Oscilloscope screen captures of modulation amplitude of a CMIT feature (upper, blue trace) at different modulation frequencies of the AOM (left: 1 MHz; center: 3 MHz; right: 4.2 MHz).

At the frequency that gives the minimum relative modulation amplitude on resonance, at the position of the central IT peak (4.2 MHz in the case of Fig. 5), we can use the relation in Eq. (4) to find another estimate of the CPC strength T_s for comparison. Note that the sinusoidal modulation of the input field amplitude is achieved by using our AOM, which has a finite response time and limits the modulation frequency to less than 10 MHz (actually the modulation signal starts to be distorted when the frequency exceeds 5 MHz). So we had to keep the modulation frequency relatively low. From the model fitting result, we estimate the range of the modulation frequency we need. If it is too large, we will skip that set of data and look for another CMIT/ATS feature that gives a modulation frequency within the safe range. Another challenge is that the presence of mode overlap in the throughput spectra made it difficult to find clear CMIT and ATS features. By using tapered fibers with different diameters, we reduced the mode density and hence minimized mode overlap of the WGMs when the tapered fiber is in contact with the HBR. For a number of cases of CMIT and ATS, we estimated the CPC strength from model fitting and observed the modulation amplitude of the input field to get another estimate of CPC strength. Table 1 compares the values of T_s from numerical fitting and from amplitude modulation at a range of modulation frequencies of the AOM.

Table 1. Comparing the values of T_s from numerical fitting and from amplitude modulation.

Modulation frequency (ν_{min} = $\Omega_{min}/2\pi$)	**CMIT or ATS**	***Q* values**	**Dip depths and Coupling regimes**	**T_s (numerical fitting)**	**T_s (amplitude modulation)**	**difference**
1.6 MHz	ATS	$Q_1 = 4.21 \times 10^6$ $Q_2 = 1.05 \times 10^7$	$M_1 = 0.78$ (undercoupled) $M_2 = 0.94$ (undercoupled)	3.16×10^{-7}	2.90×10^{-7}	8.58 %
2.5 MHz	CMIT	$Q_1 = 7.23. \times 10^6$ $Q_2 = 3.45 \times 10^8$	$M_1 = 0.94$ (undercoupled) $M_2 = 0.91$ (undercoupled)	7.23×10^{-9}	6.80×10^{-9}	6.13 %
4.2 MHz	ATS	$Q_1 = 2.18 \times 10^7$ $Q_2 = 2.74 \times 10^7$	$M_1 = 0.81$ (undercoupled) $M_2 = 0.67$ (undercoupled)	1.99×10^{-8}	1.94×10^{-8}	2.50 %
7.2 MHz	ATS	$Q_1 = 7.90 \times 10^6$ $Q_2 = 1.30 \times 10^7$	$M_1 = 0.87$ (undercoupled) $M_2 = 0.81$ (undercoupled)	6.30×10^{-8}	5.67×10^{-8}	10.53 %

The two values of CPC strength for each case agree quite well, with only a small percent difference (less than the 25% uncertainty in each T_s value). These results indicate that we have developed an independent method of estimating the CPC strength, by using sinusoidal modulation at the input.

4. DISCUSSION

We will do more CMIT/CMIA and ATS experiments to check the limitations of this new way of finding cross polarization coupling strength. Other experiments will help to confirm that the CPC effect is a result of polarization rotation. The coupling effect between orthogonally polarized modes in a single resonator can lead to CMIT/CMIA or to ATS. These effects enable slow light or fast light and have potential applications, which make it important for us to get a clear understanding of the dynamics of the CPC. Previously, the intermode coupling strength was determined by fitting the experimental throughput spectra to a Mathematica model. Now the modulation response gives us an independent way to find the value of the CPC strength T_s. Being able to determine the intermode coupling strength without model fitting may help us to get a better understanding of the dynamics of the CPC effect in microresonators. In particular, a good understanding of the exceptional point may enhance sensor applications of microresonators. We also expect other applications to be improved with the help of our dynamics study.

ACKNOWLEDGMENTS

We would like to thank: Razvan I. Stoian, for developing the HBR fabrication procedures; Khoa V. Bui, for preparing the experimental setup; and Karleyda Sandoval, for setting up a Python model for data analysis. In addition, former undergraduate student Brian Ragsdale also made contributions to the numerical analysis in this work.

REFERENCES

[1] Vahala, K. J., "Optical microcavities," Nature 424, 839-846 (2003)

[2] Fleischhauer, M., Imamoglu, A., and Marangos, J. P., "Electromagnetically induced transparency: Optics in coherent media," Rev. Mod. Phys. 77, 633-673 (2005).

[3] Rosenberger, A. T., "EIT analogs using orthogonally polarized modes of a single whispering-gallery microresonator," Proc. SPIE 8636, 863602 (2013).

[4] Autler, S. H. and Townes, C. H., "Stark effect in rapidly varying fields," Phys. Rev. 100, 703-722 (1955).

[5] Peng, B., Özdemir, Ş. K., Chen, W., Nori, F., and Yang, L., "What is and what is not electromagnetically induced transparency in whispering-gallery microcavities," Nat. Commun. 5, 5082 (2014).

[6] Smith, D. D., Chang, H., Fuller, K. A., Rosenberger, A. T., and Boyd, R. W., "Coupled resonator induced transparency," Phys. Rev. A 69, 063804 (2004).

[7] Naweed, A., Farca, G., Shopova, S. I., and Rosenberger, A. T., "Induced transparency and absorption in coupled whispering-gallery microresonators," Phys. Rev. A 71, 043804 (2005).

[8] Rosenberger, A. T., "Comparison of methods for achieving induced transparency or absorption with pulse delay or advancement in a single microresonator," Proc. SPIE 9763 (2016)

[9] Dale, E. B., *Coupling Effects in Dielectric Microcavities*, PhD dissertation, Oklahoma State University, 2010.

[10] Rosenberger, A. T., "Cross-polarization coupling of whispering-gallery modes due to the spin-orbit interaction of light," Proc. SPIE 10904 (2019), to be published.

[11] Bui, K. V., and Rosenberger, A. T., "Experimental study of induced transparency or absorption and slow or fast light using orthogonally polarized whispering-gallery modes of a single microresonator," Proc. SPIE 9763, 97630W (2016).

[12] Murugan, G. S., Petrovich, M. N., Jung, Y., Wilkinson, J. S., and Zervas, M. N., "Hollow-bottle optical microresonators," Opt. Express 19, 20773–84 (2011).

[13] Stoian, R.-I., Bui, K. V., and Rosenberger, A. T., "Silica hollow bottle resonators for use as whispering gallery mode based chemical sensors," J. Opt. 17, 125011 (2015).

[14] Bui, K. V., *Induced Transparency and Pulse Delay Plus Induced Absorption and Pulse Advancement Using the Orthogonally Polarized Whispering Gallery Modes of a Single Microresonator*, PhD dissertation, Oklahoma State University, 2016.